# Full-waveform inversion of multicomponent data for layered VTI media

Nishant Kamath & Ilya Tsvankin

*Center for Wave Phenomena, Colorado School of Mines*

**ABSTRACT**

Although full-waveform inversion (FWI) has shown significant promise in reconstructing heterogeneous velocity fields, most existing methodologies are limited to acoustic models. We extend FWI to multicomponent (PP and PS) data from anisotropic media, with the current implementation limited to a stack of horizontal, homogeneous VTI (transversely isotropic with a vertical symmetry axis) layers. The algorithm is designed to estimate the interval vertical P- and S-wave velocities ($V_{P0}$ and $V_{S0}$) and Thomsen parameters $\epsilon$ and $\delta$ from long-spread PP and PSV reflections. The forward-modeling operator is based on the anisotropic reflectivity technique, and the inversion is performed in the time domain using the gradient (Gauss-Newton) method. To build the initial model, we perform nonhyperbolic semblance analysis, which yields the zero-offset traveltimes and effective NMO velocities of PP- and PS-waves along with the anellipticity parameter $\eta$. Then the interval parameters are obtained either from Dix-type equations or velocity-independent layer stripping.

To identify the medium parameters constrained by the data we perform eigenvalue/eigenvector decomposition of the approximate Hessian matrix for a VTI layer embedded between isotropic media. Analysis of the eigenvectors shows that the objective function is weakly sensitive to density, but the parameters $V_{P0}$, $V_{S0}$, $\epsilon$, and $\delta$ can be resolved not only by joint inversion of PP and PS data, but also with PP reflections alone. Although the inversion becomes more stable with increasing spreadlength-to-depth (X/Z) ratio, the VTI model can be constrained even by PP data acquired on conventional spreads (X/Z=1). For multilayered VTI media, the sensitivity of the objective function to the interval parameters decreases with depth. Still, it is possible to resolve the VTI parameters even for the deeper layers, if the ratio X/Z for the bottom of the layer reaches two. The insights gained here by examining simple layered models should help guide the inversion for more realistic heterogeneous TI media.

## 1 INTRODUCTION

Transversely isotropic media with a vertical axis of symmetry (VTI) are described by the vertical P- and S-wave velocities, $V_{P0}$ and $V_{S0}$, and the Thomsen parameters $\epsilon$, $\delta$, and $\gamma$. However, traveltime analysis of PP-wave reflection data typically yields just the P-wave normal-moveout velocity $V_{\mathrm{nmo,P}}$ and anellipticity coefficient $\eta$ (Alkhalifah and Tsvankin, 1995):

$$V_{\mathrm{nmo},P} = V_{P0}\sqrt{1 + 2\delta}\,, \qquad (1)$$

$$\eta = \frac{\epsilon - \delta}{1 + 2\delta}\,. \qquad (2)$$

In moveout inversion, $\eta$ is often replaced with the P-wave horizontal velocity:

$$V_{\mathrm{hor},P} = V_{P0}\sqrt{1 + 2\epsilon}\,. \qquad (3)$$

Tsvankin and Thomsen (1995) show that all four parameters responsible for propagation of P- and SV-waves ($V_{P0}$, $V_{S0}$,

$\epsilon$, and $\delta$) can be obtained from long-spread PP- and SS-wave traveltimes. Shear waves, however, cannot be excited in offshore surveys and are seldom generated on land. Therefore, here we consider joint inversion of PP-waves and converted PSV modes. The replacement of pure SS reflections with PS-waves, however, complicates velocity analysis because even long-spread traveltimes of PP- and PS-waves are insufficient for constraining the interval parameters $V_{P0}$, $V_{S0}$, $\epsilon$, and $\delta$ of layer-cake VTI media (Grechka and Tsvankin, 2002).

Here, we examine the feasibility of reconstructing layered VTI models in depth using full-waveform inversion of PP and PS data. FWI can be performed either in the time domain (Kolb et al., 1986; Gauthier, 1986; Mora, 1987; Bunks et al., 1995) or frequency domain (Song and Williamson, 1995; Song et al., 1995; Pratt, 1999; Pratt and Shipp, 1999). It is typically based on gradient estimation by zero-lag crosscorrelation of the source and residual receiver wavefields, as described in Tarantola (1984). Most existing algorithms are designed for

isotropic, acoustic media, and operate primarily with diving waves. However, when the medium is anisotropic, it is highly beneficial to combine PP-wave data with PS- or SS-waves, which requires employing elastic models. Taking elasticity into account also makes it possible to properly model reflection amplitudes.

Plessix and Rynja (2010) implement FWI for VTI media in the acoustic approximation to invert for the NMO velocity $V_{\mathrm{nmo},P}$, anellipticity parameter $\eta$, and $\delta$. Plessix and Cao (2011) invert phase information contained in diving waves and near-offset reflections for the long-wavelength components of the NMO ($V_{\mathrm{nmo},P}$) and horizontal ($V_{\mathrm{hor},P}$) velocities. Single- and multi-parameter FWI for VTI media is performed by Gholami et al. (2011). In the former case, they estimate only one velocity parameter ($V_{P0}$, $V_{\mathrm{nmo},P}$, or $V_{\mathrm{hor}}$) while the long-wavelength variations of $\epsilon$ and $\delta$ are fixed at the correct values. They also invert for two velocities ($V_{\mathrm{hor},P}$ and $V_{P0}$) under the assumption that the long-wavelength spatial variation of $\delta$ are known. They conclude that the single-parameter inversion provides a good estimate of the unknown velocity, while multiparameter inversion can resolve only one of the velocities.

Chang and McMechan (2009) perform a feasibility study of FWI for a horizontal anisotropic layer sandwiched between isotropic media. In addition to transversely isotropic TI layers with a vertical (VTI) and horizontal (HTI) symmetry axis, they also consider a layer of orthorhombic symmetry. They use multicomponent data to invert for the vertical P- and S-wave velocities, anisotropy parameters, and density of the anisotropic layer as well as for the parameters of the underlying isotropic halfspace. Inversion is performed in two steps: first, reflections from the top of the anisotropic layer are used to estimate its parameters; then, the entire data set is inverted for the parameters of both the anisotropic layer and the halfspace. They conclude that wide-azimuth reflections from both the top and bottom of the anisotropic layer are needed for stable parameter estimation.

Here we develop an FWI algorithm for multicomponent data from more realistic, multilayered anisotropic media. PP and PS reflections from all interfaces are inverted simultaneously, which mitigates downward error propagation through the model. First, we describe application of moveout inversion to building the initial model from just PP-wave moveout or from the combination of PP and PS reflection traveltimes. Then we analyze the Hessian matrix for layered VTI models to identify the parameters constrained by input data acquired for a wide range of spreadlength-to-depth (X/Z) ratios. The inversion algorithm is applied separately to just PP data and to the combination of PP and PS reflections to evaluate the feasibility of building VTI depth models from different input data.

## 2    METHODOLOGY

We generate 2D synthetic PP and PS(PSV) data from a point explosive source with the anisotropic reflectivity method (Mallick and Frazer, 1990). In practice, reflection data are sorted into CMP gathers to minimize reflection-point dispersal. However, our FWI algorithm is applied to shot gathers be-

cause it operates with synthetic data from horizontally layered media. The parameters of the first layer (or the overburden) are assumed to be known and fixed at the correct values during the inversion.

### 2.1    Building the initial model

To build the initial model, we employ widely used moveout-inversion techniques. Time processing of PP reflection data in VTI media is fully controlled by the parameters $V_{\mathrm{nmo},P}$ and $\eta$, which can be estimated from PP-wave traveltimes. The PP-wave long-spread reflection moveout in a horizontal VTI layer is described by the nonhyperbolic equation of Alkhalifah and Tsvankin (1995):

$$t^2 = t_{P0}^2 + \frac{x^2}{V_{\mathrm{nmo},P}^2} - \frac{2\,\eta\,x^4}{V_{\mathrm{nmo},P}^2\left[t_0^2\,V_{\mathrm{nmo},P}^2 + (1+2\eta)\,x^2\right]},$$
(4)

where $x$ is the offset and $t_{P0}$ is the PP-wave two-way zero-offset time. The velocity $V_{\mathrm{nmo},P}$ controls the moveout on conventional spreads, while $\eta$ is responsible for deviation from hyperbolic moveout in long-spread data.

Equation 4 remains valid for layered VTI media, with $V_{\mathrm{nmo},P}$ and $\eta$ becoming effective quantities for the stack of layers above the reflector. If the spreadlength-to-depth ratio X/Z is less than 1.5, the magnitude of nonhyperbolic moveout is insufficient for constraining $\eta$. For X/Z reaching 1.5-2, equation 4 is used to perform 2D semblance scanning and estimate the effective parameters $V_{\mathrm{nmo},P}$ and $\eta$. If the offset range is wide enough to record head waves, $V_{\mathrm{hor},P}$ can be estimated directly from the head-wave moveout (Tsvankin, 2005). Then the interval velocity $V_{\mathrm{nmo},P}$ is found from the conventional Dix equation and the interval $\eta$ from the Dix-type equation given in Tsvankin (2005), Appendix 4B.

Because of the trade-off between the moveout parameters, the error in the effective $\eta$ can be substantial (Alkhalifah, 1997; Grechka and Tsvankin, 1998). In addition, the errors in the effective parameters are amplified by Dix-type differentiation. A more stable technique for estimating the interval moveout parameters is based on velocity-independent layer stripping (VILS) developed by Dewangan and Tsvankin (2006). VILS mitigates error propagation into the interval parameters even in the presence of correlated noise (Wang and Tsvankin, 2009).

The density $\rho$ and shear-wave vertical velocity $V_{S0}$ (if only PP data are available) for the initial model are supposed to be found from well logs. The initial value of $\delta$ is set to zero, which allows us to find the parameters $V_{P0}$ and $\epsilon$ from $V_{\mathrm{nmo},P}$ and $\eta$.

For multicomponent data, it is necessary to identify the PP and PS (PSV) reflections from the same interfaces (i.e., perform event registration). The interval values of $V_{\mathrm{nmo},P}$ and $\eta$ can be calculated from P-wave data as described above. To estimate the effective PS-wave NMO velocity ($V_{\mathrm{nmo},PS}$), we apply a 2D semblance scan based on equation 4 to long-spread PS data. In this case, $\eta$ represents just a fitting parameter, but the equation is sufficiently accurate to constrain $V_{\mathrm{nmo},PS}$,

which replaces $V_{\text{nmo},P}$ in equation 4 (Xu and Tsvankin, 2008). Then the effective NMO velocity $V_{\text{nmo},SV}$ of the pure SS reflection can be found from (Seriff and Sriram, 1991):

$$2t_{PS0}V_{\text{nmo},PS}^2 = t_{P0}V_{\text{nmo},P}^2 + t_{S0}V_{\text{nmo},SV}^2, \qquad (5)$$

where $t_{PS0}$ and $t_{S0}$ are the zero-offset traveltimes of PS- and SS-waves respectively, so

$$t_{S0} = 2t_{PS0} - t_{P0}. \qquad (6)$$

The SV-wave NMO velocity is given by (Tsvankin, 2005):

$$V_{\text{nmo},SV} = V_{S0}\sqrt{1 + 2\sigma}, \qquad (7)$$

where

$$\sigma = \left(\frac{V_{S0}}{V_{S0}}\right)^2 (\epsilon - \delta). \qquad (8)$$

The NMO velocities $V_{\text{nmo},P}$ and $V_{\text{nmo},SV}$ and the vertical-velocity ratio $V_{P0}/V_{S0} = t_{S0}/t_{P0}$ are generally well-constrained by reflection traveltimes. Grechka and Tsvankin (2002) show that in principle it is possible to calculate all four parameters ($V_{P0}, V_{S0}, \epsilon,$ and $\delta$) from $V_{\text{nmo},P}$, $V_{\text{nmo},SV}$, $V_{P0}/V_{S0}$, and $\eta$. The parameter $\delta$ can be found from

$$1 + 2\delta = \left(\frac{t_{P0}}{t_{S0}}\right)^2 \frac{1}{(V_{\text{nmo},SV}/V_{\text{nmo},P})^2 - 2\eta}. \qquad (9)$$

Then, $V_{P0}$ and $\epsilon$ are obtained from equations 1 and 2 and $V_{S0}$ from the ratio $t_{S0}/t_{P0}$. However, small errors in the NMO velocities and $\eta$ lead to large errors in the estimated $\delta$, which propagate into the other VTI parameters and make the results too unstable for accurate model-building (Grechka and Tsvankin, 2002). Still, this approach provides us with an initial model to be updated by full-waveform inversion.

## 2.2 Inversion algorithm

We perform time-domain inversion of either PP data alone or the combination of PP and PS reflections. The least-squares objective function is defined as:

$$\mathcal{F}(\mathbf{m}) = \frac{1}{2}\|\mathbf{d}_{\text{obs}} - \mathbf{d}_{\text{cal}}(\mathbf{m})\|^2, \qquad (10)$$

where $\mathbf{d}_{\text{obs}}$ is the observed data and $\mathbf{d}_{\text{cal}}(\mathbf{m})$ is the data calculated for a certain model $\mathbf{m}$. The model updating is carried out via the Gauss-Newton method,

$$(\mathbf{\Delta m}) = [\mathbf{J^T J}]^{-1}\mathbf{J^T \Delta d}, \qquad (11)$$

where $\mathbf{J}$ is the Fréchet derivative matrix obtained by perturbing each model parameter, $\mathbf{J^T J}$ is the approximate Hessian, and $\mathbf{\Delta d}$ is the difference between the observed data and those computed for a trial model. Forward modeling is carried out with the anisotropic reflectivity algorithm of Mallick and Frazer (1990), based on the formulation introduced by Fryer and Frazer (1984). The main advantage of this method is that it produces the exact reflected wavefield for horizontally layered media including all multiples and mode conversions. In addition, it is possible to separate the wavefield and model either just PP reflections or both PP and mode-converted PS data.

Since the vertical velocities and anisotropy parameters do not have the same units, it is more convenient to invert for the vertical and NMO velocities. If only PP data are used, each layer is described by the parameters $V_{P0}$, $V_{\text{nmo},P}$, $V_{\text{hor},P}$, $V_{P0}/V_{S0}$, and the density $\rho$. In the case of joint inversion of PP and PS data, we etimate the interval values of $V_{P0}$, $V_{S0}$, $V_{\text{nmo},P}$, $V_{\text{nmo},SV}$, and $\rho$. The initial values of $V_{P0}$ and $V_{S0}$ obtained from PP and PS data can be used to calculate the initial $V_{P0}/V_{S0}$ ratio for the inversion of PP-waves. In practice, if only PP reflections are acquired, the initial $V_{P0}/V_{S0}$ has to be known a priori (e.g., from well logs).

## 2.3 Amplitude signature of P-waves

The inversion algorithm is designed to fit both amplitudes and phase of the modeled data (as part of the full waveforms) to those of the recorded wavefield. The dependence of traveltimes on the parameters of layered VTI media was discussed above. Next, we briefly describe the influence of anisotropy on reflection coefficients and geometrical spreading of PP-waves.

The PP-wave reflection coefficient at a boundary between VTI halfspaces in the weak-contrast, weak-anisotropy ($|\delta| \ll 1$, $|\epsilon| \ll 1$) approximation is given by (Rüger, 1997, 2002):

$$R = \frac{1}{2}\frac{\Delta Z}{\overline{Z}} + \frac{1}{2}\left[\frac{\Delta V_{P0}}{\overline{V}_{P0}} - \left(\frac{2\overline{V}_{S0}}{V_{P0}}\right)^2 \frac{\Delta G}{\overline{G}} + \Delta\delta\right]\sin^2\theta$$
$$+ \frac{1}{2}\left[\frac{\Delta V_{P0}}{\overline{V}_{P0}} + \Delta\delta\right]\sin^2\theta\tan^2\theta, \qquad (12)$$

where $\theta$ is the incidence phase angle, $Z = \rho V_{P0}$ is the PP-wave vertical impedance, and $G = \rho V_{S0}^2$ is the S-wave vertical rigidity modulus. The difference between the parameter B below and above the reflector is denoted by $\Delta B = B_2 - B_1$. The average of the two parameters is denoted by $\overline{B} = (B_1 + B_2)/2$.

The first term in equation 12 is the normal-incidence reflection coefficient, also known as the AVO intercept, which is equal to the fractional difference between the impedances in the two media. The second term is responsible for amplitude variation near the vertical and is called the AVO gradient. It depends on the jumps in $V_{P0}$ and G across the interface and on the contrast in the parameter $\delta$. Hence, PP-wave reflection data at small offsets ought to be sensitive to those parameters; note that G depends on the shear-wave velocity $V_{S0}$. The third term contributes to the amplitude variation at large offsets and is called the "curvature term."

The far-field amplitude of the PP-wave excited by a point force in a homogeneous, weakly anisotropic TI medium is given by (Tsvankin, 1995, 2005; Xu et al., 2005):

$$A_P(R,\theta) = \frac{F_u}{4\pi\rho V_{P0}^2 R}\frac{1 - 2(\epsilon - \delta)\sin^2 2\theta + \delta\sin^2\theta}{1 + 2\delta}, \qquad (13)$$

where $F_u$ is the projection of the force $\mathbf{F}$ onto the polarization vector, $R$ is the source-receiver distance, and $\theta$ is the phase angle with the symmetry axis. For small angles $\theta$, the amplitude variation with angle is largely controlled by $\eta \approx \epsilon - \delta$,
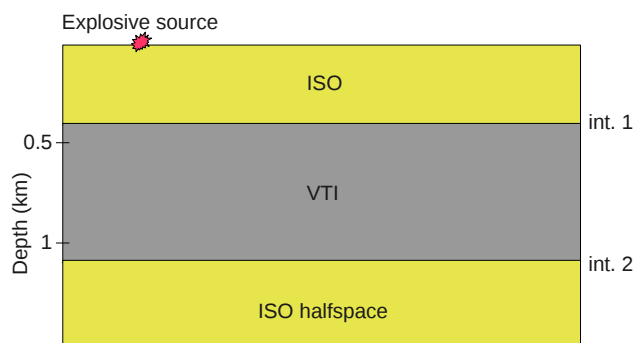
**Figure 1.** Three-layer model used in the tests. The parameters of the top isotropic layer are $V_P = 2800$ m/s, $V_S = 1400$ m/s, and $\rho = 1.8$ g/cm$^3$. For the VTI layer, $V_{P0} = 3000$ m/s, $V_{S0} = 1632$ m/s, $\epsilon = 0.25$, $\delta = 0.1$, and $\rho = 2.4$ g/cm$^3$. For the bottom halfspace, $V_P = 3400$ m/s, $V_S = 1800$ m/s, and $\rho = 3.2$ g/cm$^3$.

which has important implications for our FWI results. Although equation 13 is derived for a homogeneous medium, it also describes the behavior of the anisotropic geometrical-spreading factor in any TI layer crossed by the reflected ray (Tsvankin, 2005).

## 3   INVERSION RESULTS

First, the FWI algorithm is applied to the simple three-layer model in Figure 1. The top layer is isotropic, and its velocities and density are assumed to be known. The bottom halfspace is also known to be isotropic, but its parameters are estimated by FWI. We perform tests for data with the spreadlength-to-depth ratio X/Z ranging from one to three. For X/Z=1, as mentioned before, $\eta$ cannot be constrained by PP reflection traveltimes, so the initial values of $\epsilon$ and $\delta$ are set to zero. For larger spreads (X/Z=1.5, 2, and 3), inversion is performed with the initial $\delta$ either set to zero, or (when PS data are included) computed from equation 9. For PP data, the initial value of $\epsilon$ is then obtained from $\eta$, and the initial $V_{P0}$ from $V_{\text{nmo},P}$ (equations 1 and 2).

The testing shows that the interval parameters $V_{P0}$, $V_{S0}$, $\epsilon$, and $\delta$ can be constrained by FWI, but the inversion is extremely sensitive to the starting model when the data include both PP and PS reflections. When PP and PS data are inverted with the initial $\delta = 0$, the algorithm converges to the correct values only for X/Z=1. For longer spreads, accurate inversion requires calculating $\delta$ from equation 9, even though that equation produces errors reaching 0.6. This is likely due to the shape of the objective function, which causes the inversion for the initial $\delta = 0$ to get trapped in local minima.

To evaluate the sensitivity of the objective function to the model parameters, we perform the eigenvector/eigenvalue decomposition of the Hessian matrix for joint inversion of PP and PS data (Plessix and Cao, 2011). Each component of an eigenvector (called the "direction cosine") indicates the relative sensitivity of the objective function to the model parame-
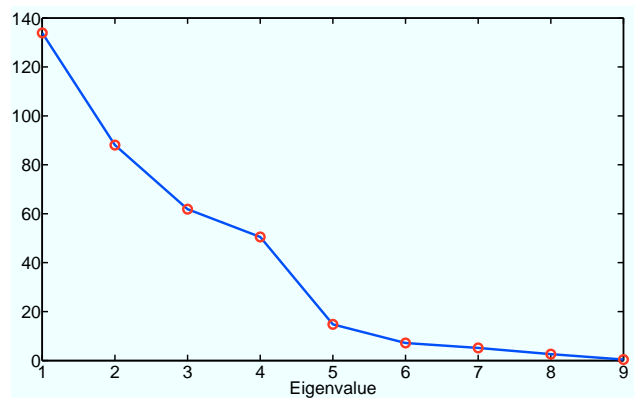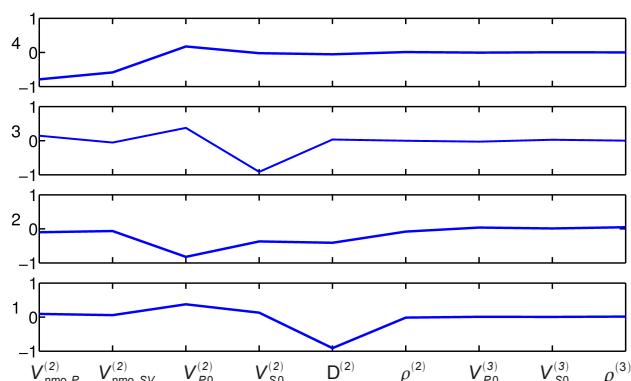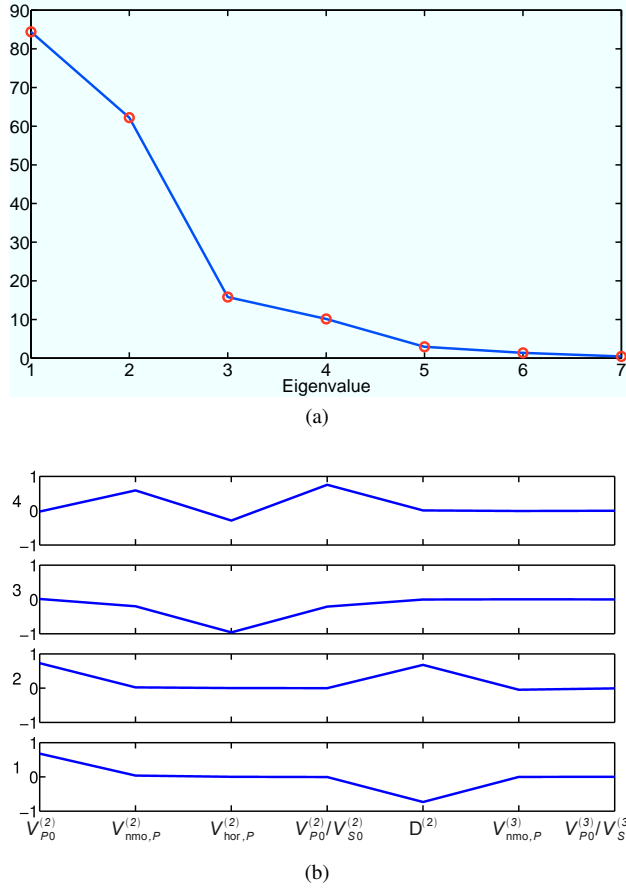


**Figure 2.** (a) Eigenvalues of the Hessian matrix. (b) Components of the eigenvectors (numbered 1 to 4) associated with the four largest eigenvalues of the Hessian. The input data include PP and PS reflections for the model in Figure 1 for X/Z=1.5. The superscript (2) denotes the VTI layer and (3) the bottom isotropic halfspace. The layer thickness is denoted by D.

ters. Figure 2(b) shows that the objective function is most sensitive to the layer thickness D (and hence to $V_{P0}$, since the vertical traveltimes are well-constrained), followed by $V_{S0}$, $V_{\text{nmo},P}$, and $V_{\text{nmo},SV}$. This result is in agreement with Plessix and Cao (2011), who showed that for small-offset P-wave reflected data, the objective function is highly sensitive to the velocity $V_{P0}$. In contrast, all our tests demonstrate that the objective function is weakly sensitive to density. Although the densities change at every iteration, the inversion gets trapped in local minima. Apparently, the objective function becomes much more complicated with the inclusion of density as an unknown parameter. Hence, in all subsequent tests the interval densities are fixed at the correct values.

Next, we generate only PP data for the same model and invert for the parameters $V_{P0}$, $V_{\text{nmo},P}$, $V_{\text{hor},P}$, and $V_{P0}/V_{S0}$ using the same range of spreadlengths. For all values of X/Z, the algorithm converges to the correct parameters even when the initial value of $\delta$ is set to zero. Evidently, the objective
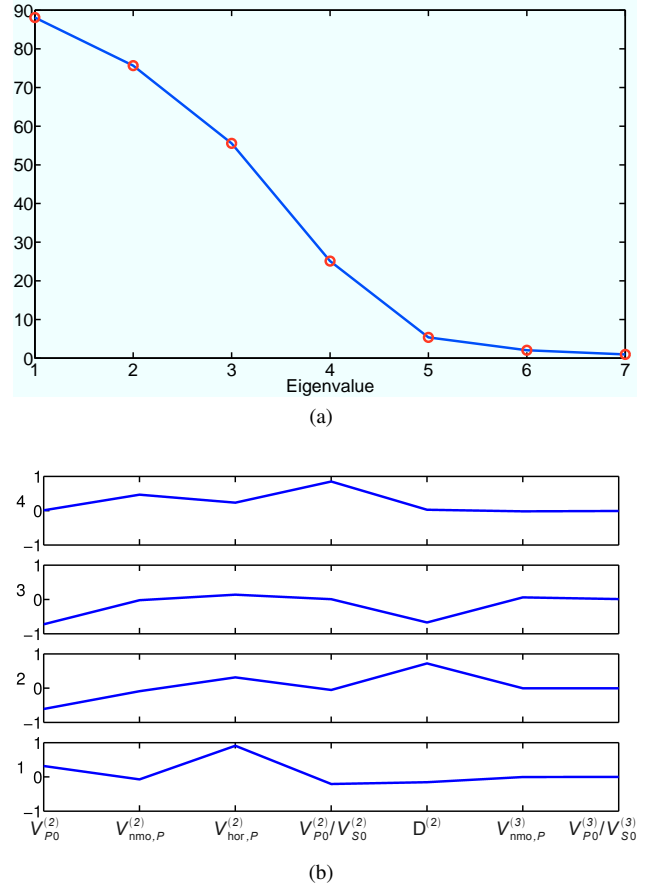
(a)



(b)

**Figure 3.** (a) Eigenvalues of the Hessian matrix and (b) the components of the eigenvectors (numbered 1 to 4) associated with the four largest eigenvalues of the Hessian. The input data include PP reflections for the model in Figure 1 for X/Z=1.



(a)



(b)

**Figure 4.** (a) Eigenvalues of the Hessian matrix and (b) the components of the eigenvectors (numbered 1 to 4) associated with the four largest eigenvalues of the Hessian. The input data include PP reflections for the model in Figure 1 for X/Z=2. The data are contaminated with band-limited (10-25 Hz) random noise; the signal-to-noise ratio is five.

function has a simpler shape with fewer local minima, if only PP data are included.

Interestingly, for X/Z=1 the inversion yields accurate results despite the absence of PS data. This is an unexpected result since such spreadlengths are not sufficient to constrain the horizontal velocity (or the parameter $\eta$) and, therefore, $\epsilon$ using reflection traveltimes. However, equation 13 indicates that the geometrical-spreading factor near the symmetry axis is sensitive to $\eta$, which helps estimate all VTI parameters using full-waveform data. Therefore, FWI of PP reflections can reconstruct the depth scale of simple layer-cake models even without including long-offset data.

For PP data, the eigenvectors associated with the two largest eigenvalues of the Hessian (Figure 3b) point equally in the direction of two model parameters ($V_{P0}$ and D), and so the objective function is sensitive to the combination of $V_{P0}$ and D. The third eigenvector, on the other hand, points almost entirely in the direction of $V_{\mathrm{hor},P}$. As mentioned above, the near-offset P-wave amplitude is influenced by $\eta$, which may help resolve $V_{\mathrm{hor},P}$. The objective function for PP-wave in-

version is not as sensitive to the $V_{P0}/V_{S0}$ ratio as it is to $V_{P0}$ and D. Indeed, the exact P-wave geometrical-spreading factor in the $0° − 40°$ range typically changes by less than 2-3% for the $V_{P0}/V_{S0}$ ratio varying from 1.73 to 2.2 (Tsvankin, 2005). However, the P-wave AVO gradient (and the P-wave reflection coefficient as a whole) includes the jump in the rigidity modulus G (equation 12), which creates a dependence of the FWI objective function on $V_{S0}$.

When larger offsets are included, the velocity $V_{\mathrm{hor},P}$ (or $\eta$) is well-resolved even in the presence of random noise because it governs the magnitude of nonhyperbolic moveout (Figures 4 and 5). Indeed, for X/Z=2 the eigenvector associated with the largest eigenvalue of the Hessian points almost entirely in the direction of $V_{\mathrm{hor},P}$ (Figure 4b). The small errors (up to 0.02) in the inverted parameters $\epsilon$ and $\delta$ (Figure 5) are mostly related to the distortion in the vertical velocity $V_{P0}$.

In our inversion we assign equal weights to the horizontal and vertical displacement components. For P-waves recorded on conventional spreads, the largest eigenvalues of the Hes-
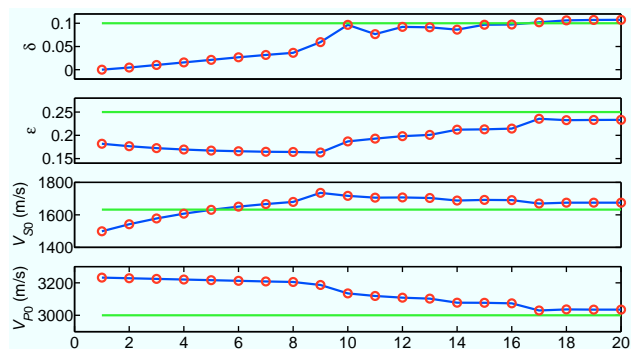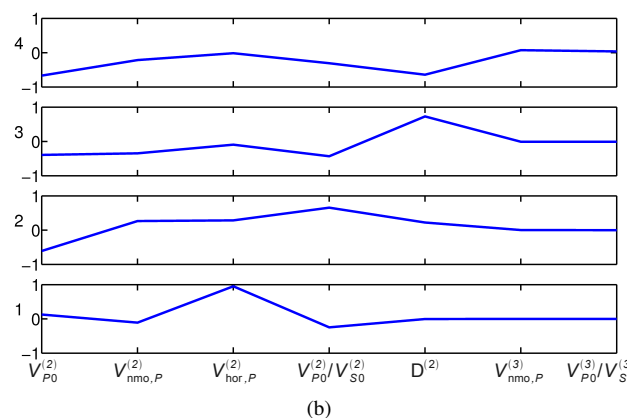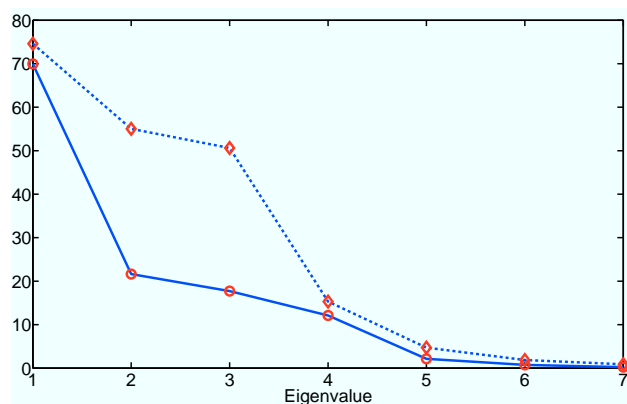
**Figure 5.** Parameters of the VTI layer (circles) after each iteration of FWI. The actual values are marked by the horizontal solid lines. The input data include PP reflections for the model in Figure 1 for X/Z=2. The data are contaminated with band-limited (10-25 Hz) random noise; the signal-to-noise ratio is five.
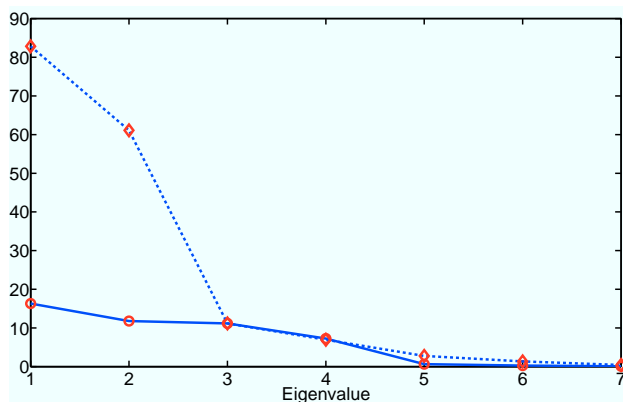


**Figure 6.** Eigenvalues of the Hessian matrices associated with the horizontal component (circles) and the vertical component (diamonds). The input data include PP reflections for the model in Figure 1 for X/Z=1.



(a)



(b)

**Figure 7.** (a) Eigenvalues of the Hessian matrices associated with the horizontal component (circles) and the vertical component (diamonds). (b) Components of the eigenvectors (numbered 1 to 4) associated with the four largest eigenvalues of $\mathbf{H}_x$. The input data include PP reflections for the model in Figure 1 for X/Z=2. The data are contaminated with band-limited (10-25 Hz) random noise; the signal-to-noise ratio is five.

sian associated with the horizontal component ($\mathbf{H}_x$) are much smaller than those for the vertical component ($\mathbf{H}_z$) (Figure 6). Hence, as expected, the objective function for P-wave inversion on conventional spreads is more sensitive to the vertical displacement. However, for a longer spread (X/Z=2), the largest eigenvalues of $\mathbf{H}_x$ and $\mathbf{H}_z$ become comparable (Figure 7(a)). In addition, the largest eigenvalue of $\mathbf{H}_x$ is three times or more the other eigenvalues, and the corresponding eigenvector points in the direction of $V_{\text{hor},P}$ (Figure 7(b)). Therefore, assigning a larger weight to the horizontal component in the objective function for long spreads may result in a faster convergence toward the correct velocity $V_{\text{hor},P}$.

Next, we test the algorithm on PP and PS data for a more complicated multilayered VTI model (Figure 8). Again, the parameters of the top layer are fixed at the correct values, and the bottom half-space is known to be isotropic. The results indicate that convergence toward the correct parameters

is strongly dependent on the initial model. If the initial value of $\delta$ is set to zero in each layer (which causes a maximum error in $\delta$ of 0.25) the inversion of PP and PS data gets trapped in local minima. However, if only PP data are inverted, the objective function apparently has a simpler shape (as was the case for the first model), and the algorithm converges toward the correct parameters. In the remaining tests, we focus on PP-wave inversion because accurate parameter estimation for the horizontally layered VTI models considered here can typically be accomplished without using PS-waves.

We contaminate PP data with band-limited (10-25 Hz) random noise, as before. The eigenvector/eigenvalue decomposition of the Hessian matrix indicates that the objective function is most sensitive to the parameters $V_{P0}$, $V_{\text{hor},P}$, and D of the shallow VTI layer and to the P-wave velocity in the isotropic layer immediately below it. The influence of the parameters of the deeper layers on the objective function is much weaker.
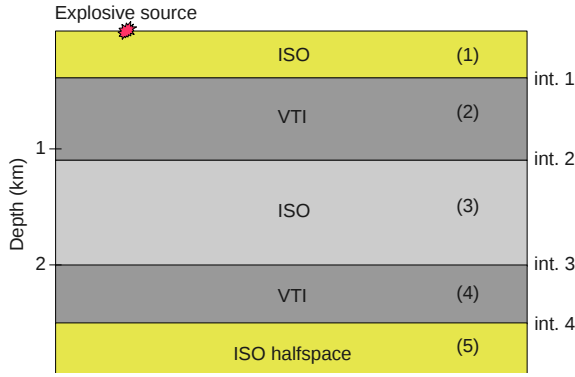
**Figure 8.** Model with two VTI layers sandwiched between isotropic media. The parameters of layer 1 are $V_P = 2800$ m/s, $V_S = 1400$ m/s, and $\rho = 1.8$ gm/cm$^3$; for layer 2, $V_{P0} = 3000$ m/s, $V_{S0} = 1632$ m/s, $\epsilon = 0.1$, $\delta = -0.05$, and $\rho = 2.1$ gm/cm$^3$; for layer 3, $V_P = 3400$ m/s, $V_S = 1800$ m/s, and $\rho = 2.4$ gm/cm$^3$; for layer 4, $V_{P0} = 3700$ m/s, $V_{S0} = 2000$ m/s, $\epsilon = 0.25$, $\delta = 0.1$, and $\rho = 2.8$ gm/cm$^3$; and for the bottom halfspace, $V_P = 4300$ m/s, $V_S = 2200$ m/s, and $\rho = 3.1$ gm/cm$^3$.
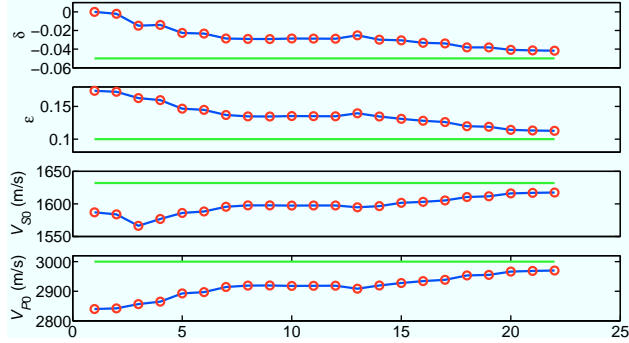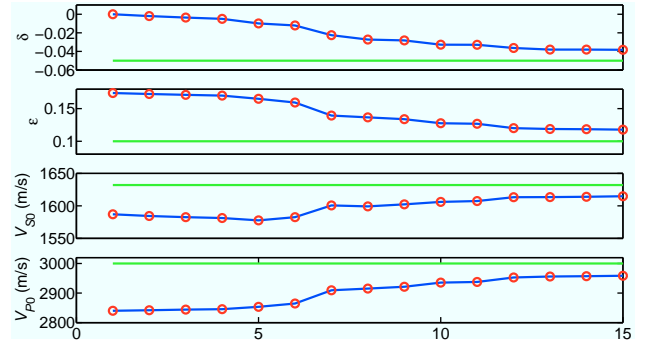


**Figure 9.** Parameters of layer 2 from the model in Figure 8 after each iteration. The input data include PP reflections; the spreadlength-to-depth ratio for the bottom of layer 2 is $X/Z_2 = 2.2$ (for the bottom of the model, $X/Z_4 = 1$). The data are contaminated with band-limited (10-25 Hz) random noise; the signal-to-noise ratio is 14.

When the spreadlength is equal to the depth of the bottom of the model, the spreadlength-to-depth ratio for the bottom of shallow VTI layer ($X/Z_2$) is close to 2.2. Then the parameters of that layer are well-constrained (Figure 9), but there are significant errors for the deeper VTI layer (Figure 10).

However, for longer spreads (the ratio $X/Z_4$ for the bottom of the model is equal to two), the parameters of the deeper VTI layer are accurately resolved (Figure 12). Therefore, when data include sufficiently long offsets (which may not be typical in practice), it is possible to invert for $V_{P0}$, $V_{S0}$, $\epsilon$, and $\delta$ with only PP-waves. Even in the presence of band-limited random noise with a signal-to-noise ratio of 14, the error in $V_{P0}$ for the deeper VTI layer is less than 2.2% for $X/Z_4 = 2$, and the errors in $\epsilon$ and $\delta$ do not exceed 0.03. Per-
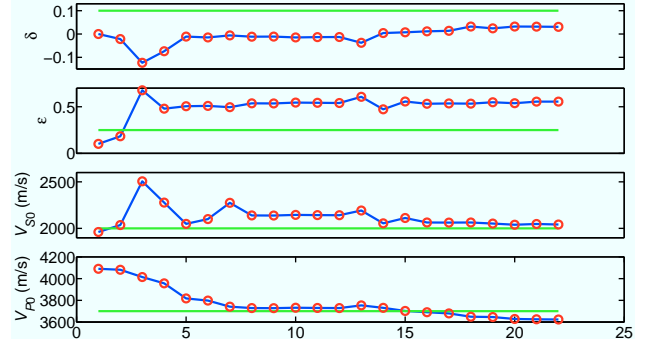


**Figure 10.** Parameters of layer 4 from the model in Figure 8 after each iteration. The input data include PP reflections; the spreadlength-to-depth ratio for the bottom of the model, $X/Z_4 = 1$. The data are contaminated with band-limited (10-25 Hz) random noise; the signal-to-noise ratio is 14.



**Figure 11.** Parameters of layer 2 from the model in Figure 8 after each iteration. The input data include PP reflections; the spreadlength-to-depth ratio $X/Z_2 \approx 4.5$ (for the bottom of the model, $X/Z_4 = 2$). The data are contaminated with band-limited (10-25 Hz) random noise; the signal-to-noise ratio is 14.
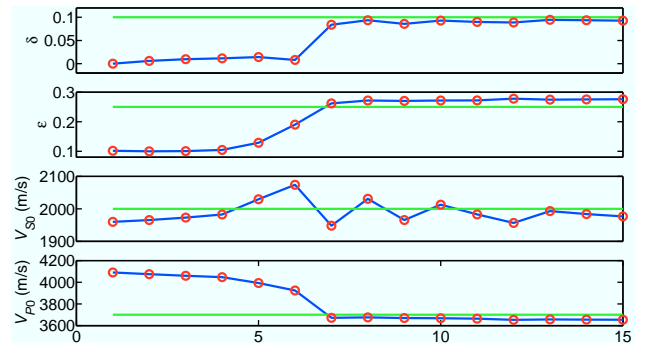


**Figure 12.** Parameters of layer 4 from the model in Figure 8 after each iteration. The input data include PP reflections; the spreadlength-to-depth ratio for the bottom of the model $X/Z_4 = 2$. The data are contaminated with band-limited (10-25 Hz) random noise; the signal-to-noise ratio is 14.

forming isotropic FWI for a VTI media, on the other hand, can lead to depth stretching or overestimation of velocity in the deeper layers (Gholami et al., 2011).

## 4    CONCLUSIONS

It is well known that the depth scale of horizontally layered VTI models is not constrained by reflection traveltimes of PP- and PS-waves, even if long-spread data are acquired. Here, we show that the interval vertical P- and S-wave velocities and anisotropy parameters $\epsilon$ and $\delta$ of layer-cake VTI media can be estimated by full-waveform inversion of PP and PS reflection data.

The gradient-based inversion algorithm operates in the time domain with PP reflections or with the combination of PP-waves and mode-converted PS-waves. Modeling is carried out with the anisotropic reflectivity method, which generates the exact multicomponent wavefield for 1D anisotropic media. The initial model for FWI is obtained from nonhyperbolic moveout inversion followed by kinematic layer stripping. It should be emphasized that our FWI algorithm estimates the parameters of all layers simultaneously to mitigate downward error propagation.

First, we examine the inversion for a single VTI layer sandwiched between isotropic layers. If the densities are fixed at the correct values, the parameters $V_{P0}$, $V_{S0}$, $\epsilon$, and $\delta$ are well-constrained by PP-waves alone. Interestingly, PP data help resolve the interval parameters even for conventional spreadlengths (X/Z=1). While PP-wave small-offset traveltimes are controlled by $V_{P0}$ and $\delta$, the geometrical-spreading factor near the symmetry axis depends on $\eta \approx \epsilon - \delta$. Still, it might be beneficial to use multicomponent data (PP and PS) data if the level of noise is high.

We also apply FWI to noise-contaminated data from a multilayered VTI model. The sensitivity of the objective function to the interval parameters decreases for the deeper layers. However, if the ratio X/Z for the bottom of the deepest VTI layer reaches two, its parameters can be obtained from the inversion of PP data.

The analysis performed here for stratified VTI media can be generalized for vertical symmetry planes of azimuthally anisotropic models (e.g., orthorhombic). However, geometrical spreading in the symmetry planes of orthorhombic media is influenced by azimuthal velocity variations and has to be modeled with a 3D algorithm. Our inversion algorithm based on the gauss-Newton method cannot be directly extended to laterally heterogeneous media. Still, the results of 1D inversion provide useful insights for designing the inversion operator capable of handling more complicated heterogeneous structures.

## 5    ACKNOWLEDGMENTS

## REFERENCES

Alkhalifah, T., 1997, Velocity analysis using nonhyperbolic moveout in transversely isotropic media: Geophysics, **62**, 1839–1854.

Alkhalifah, T., and I. Tsvankin, 1995, Velocity analysis for transversely isotropic media: Geophysics, **60**, 1550–1566.

Bunks, C., F. M. Saleck, S. Zaleski, and G. Chavent, 1995, Multiscale seismic waveform inversion: Geophysics, **60**, 1457–1473.

Chang, H., and G. McMechan, 2009, 3D 3-C full-wavefield elastic inversion for estimating anisotropic parameters: A feasibility study with synthetic data: Geophysics, **74**, WCC159–WCC175.

Dewangan, P., and I. Tsvankin, 2006, Velocity-independent layer stripping of PP and PS reflection traveltimes: Geophysics, **71**, U59–U65.

Fryer, G. J., and L. N. Frazer, 1984, Seismic waves in stratified anisotropic media: Geophysical Journal of the Royal Astronomical Society, **78**, 691–710.

Gauthier, O., 1986, Two-dimensional nonlinear inversion of seismic waveforms: Numerical results: Geophysics, **51**, 1387–1403.

Gholami, Y., R. Brossier, S. Operto, V. Prieux, A. Ribodetti, and J. Virieux, 2011, Two-dimensional acoustic anisotropic (VTI) full waveform inversion: The valhall case study: SEG Technical Program Expanded Abstracts, **30**, 2543–2548.

Grechka, V., and I. Tsvankin, 1998, Feasibility of nonhyperbolic moveout inversion in transversely isotropic media: Geophysics, **63**, 957–969.

——, 2002, The joint nonhyperbolic moveout inversion of PP and PS data in VTI media: Geophysics, **67**, 1929–1932.

Kolb, P., F. Collino, and P. Lailly, 1986, Pre-stack inversion of a 1-D medium: Proceedings of the IEEE, **74**, 498–508.

Mallick, S., and L. N. Frazer, 1990, Computation of synthetic seismograms for stratified azimuthally anisotropic media: Journal of Geophysical Research, **95**, PP. 8513–8526.

Mora, P., 1987, Nonlinear two-dimensional elastic inversion of multioffset seismic data: Geophysics, **52**, 1211–1228.

Plessix, R., and Q. Cao, 2011, A parametrization study for surface seismic full waveform inversion in an acoustic vertical transversely isotropic medium: Geophysical Journal International, **185**, 539–556.

Plessix, R., and H. Rynja, 2010, VTI full waveform inversion: a parameterization study with a narrow azimuth streamer data example: , 962–966.

Pratt, R. G., 1999, Seismic waveform inversion in the frequency domain; part 1, theory and verification in a physical scale model: Geophysics, **64**, 888–901.

Pratt, R. G., and R. M. Shipp, 1999, Seismic waveform inversion in the frequency domain; part 2; fault delineation in sediments using crosshole data: Geophysics, **64**, 902–914.

Rüger, A., 1997, P-wave reflection coefficients for trans-

versely isotropic models with vertical and horizontal axis of symmetry: Geophysics, **62**, 713–722.

———, 2002, Reflection coefficients and azimuthal avo analysis in anisotropic media: Society of Exploration Geophysicists.

Seriff, A. J., and K. Sriram, 1991, P-SV reflection moveouts for transversely isotropic media with a vertical symmetry axis: Geophysics, **56**, 1271–1274.

Song, Z., and P. R. Williamson, 1995, Frequency-domain acoustic-wave modeling and inversion of crosshole data; part 1, 2.5-D modeling method: Geophysics, **60**, 784–795.

Song, Z., P. R. Williamson, and R. G. Pratt, 1995, Frequency-domain acoustic-wave modeling and inversion of crosshole data; part II, inversion method, synthetic experiments and real-data results: Geophysics, **60**, 796–809.

Tarantola, A., 1984, Inversion of seismic reflection data in the acoustic approximation: Geophysics, **49**, 1259–1266.

Tsvankin, I., 1995, Body-wave radiation patterns and AVO in transversely isotropic media: Geophysics, **60**, 1409–1425.

———, 2005, Seismic signatures and analysis of reflection data in anisotropic media, second ed.: Elsevier.

Tsvankin, I., and L. Thomsen, 1995, Inversion of reflection traveltimes for transverse isotropy: Geophysics, **60**, 1095–1107.

Wang, X., and I. Tsvankin, 2009, Estimation of interval anisotropy parameters using velocity-independent layer stripping: Geophysics, **74**, WB117–WB127.

Xu, X., and I. Tsvankin, 2008, Moveout-based geometrical-spreading correction for ps-waves in layered anisotropic media: Journal of Geophysics and Engineering, **5**, 195–202.

Xu, X., I. Tsvankin, and A. Pech, 2005, Geometrical spreading of P-waves in horizontally layered, azimuthally anisotropic media: Geophysics, **70**, D43–D53.